

Large-Eddy-simulation analysis of airflows and strong wind hazards in urban areas



Tetsuya Takemi^{a,*}, Toshiya Yoshida^a, Mitsuaki Horiguchi^a, Wim Vanderbauwhede^b

^a Disaster Prevention Research Institute, Kyoto University, Uji, Kyoto, Japan

^b School of Computing Science, University of Glasgow, Glasgow, United Kingdom

ARTICLE INFO

Keywords:

Turbulence
Computational fluid dynamics
Large-eddy simulation
Urban hazard
Urban disaster

ABSTRACT

Understanding the characteristics of urban airflows with complex geometrical features is very important from viewpoints of assessing strong wind hazards in the region. This study investigated turbulent airflows and strong wind hazards in an urban area by conducting large-eddy simulations (LESs) with explicit representations of buildings and structures. A business district, including historical architectures, of Kyoto City was chosen. The sensitivity experiments with realistic and idealized building arrangements indicated that the actual, complicated arrangement of buildings as well as the building height variability would enhance an unsteady nature of airflows in urban canopy. An analysis of strong wind hazards under a typhoon condition shows that sustained winds are stronger along streamwise-oriented major streets and over open spaces while instantaneous winds become stronger especially within areas with a mixture of high-rise buildings embedded in low-rise building areas/open spaces. It was indicated that wind gustiness increases with the decrease in building plane-area index. The analysis suggested that both the building height variability and the complex arrangement of buildings are considered to enhance the gustiness of surface winds. This study demonstrated that an LES model is practically useful for assessing the strong wind hazards in urban areas.

1. Introduction

Airflows in urban and/or populated areas determine the environmental conditions for our daily lives and activities. With the advances of urbanization, there are serious environmental problems such as urban heat island and air pollution. In addition, strong winds during the landfall of tropical cyclones are a great threat to human lives, social infrastructures, and economic activities in urban areas. With complex geometrical features of urban areas, the spatiotemporal variability of winds becomes high and wind gusts will be severer, which is regarded as a strong wind hazard that may lead to disasters. Furthermore, impacts of climate change on tropical cyclone hazards are of great concern to our society and thus have been extensively investigated in a number of recent studies (Hill and Lackmann, 2011; Lackmann, 2015; Tsuboki et al., 2015; Takemi et al., 2016a, 2016b, 2016c; Ito et al., 2016; Kanada et al., 2017a, 2017b; Nayak and Takemi, 2019a, 2019b). In this way, understanding the characteristics of airflows in urban areas is very important from viewpoints of assessing strong wind hazards in the region.

Airflows in urban areas are more complex than the boundary-layer flows over natural and flat grounds with no significant surface roughness and terrain undulation (Belcher, 2005; Fernando, 2010; Fernando et al., 2010). Bottema (1997) demonstrated the presence of roughness sublayer below the surface inertial layer. In this roughness sublayer, the vertical gradient of wind speed becomes smaller

* Corresponding author at: Disaster Prevention Research Institute, Kyoto University, Gokasho, Uji, Kyoto 611-0011, Japan.

E-mail address: takemi@storm.dpri.kyoto-u.ac.jp (T. Takemi).

than that in the inertial layer, which is due to the enhanced vertical mixing of momentum by the presence of roughness obstacles. The flow patterns over roughness obstacles that mimic urban rough surfaces were investigated in idealized settings by laboratory and numerical experiments (e.g., Hussain and Lee, 1980; Oke, 1988; Shao and Yang, 2005), focusing on the influences of the density of roughness obstacles on flow structures. Wieringa (1993) showed that the vertical profiles of winds critically depend on different flow regimes. Furthermore, three dimensional features of the roughness arrangements also affect airflow patterns (Oke, 1988; Hunter et al., 1990). Such complex flow patterns were also theoretically and analytically examined in detail (Raupach, 1992; MacDonald et al., 1998; Shao and Yang, 2008). For cases in actual urban areas, Grimmond and Oke (1999) examined the relationships of the roughness density in urban areas with the roughness parameters and showed that the roughness length increases with the increase in roughness density up to some point but decreases with the further increase in roughness density, like those seen in the flow pattern shown in Oke (1988).

However, the geometrical features of roughness surfaces in actual cities are so complex and complicated that the assumption of constant obstacle height, commonly employed in laboratory and numerical experiments, is not valid. Understanding how the variability of the height and distribution of buildings as seen in actual urban areas affects the urban airflows has been a challenging topic (e.g., Cheng and Castro, 2002; Kanda, 2006; Xie et al., 2008; Bou-Zeid et al., 2009; Nakayama et al., 2011; Zaki et al., 2011; Kanda et al., 2013; Park et al., 2015; Giometto et al., 2016; Nakayama et al., 2016; Castro, 2017; Han et al., 2017; Xu et al., 2017; Zhu et al., 2017; Li et al., 2018; Yoshida et al., 2018; Yoshida and Takemi, 2018; Hertwig et al., 2019).

Under such urban geometrical influences, strong winds caused by tropical cyclones pose a great threat to urban areas. With this recognition, there are some studies on the urban impacts of tropical cyclones. From special observations, Kato et al. (1992) showed that gust factors during typhoons exceed 2 within urban canopy layers. From numerical simulations, Nakayama et al. (2012) estimated the gust factors in a business district of Tokyo exceeding 2 during a typhoon landfall. Estimations on surface-level winds in urban areas have also been examined. For example, Knight and Khalid (2015) used a surface friction analysis method incorporating building geometrical data to assess the impacts of hurricane winds in an urban area. Alford et al. (2019) used radar data to estimate near-surface winds by assuming a logarithmic wind profile assumption during a hurricane landfall. As a case study of an extreme wind event, Takemi et al. (2019) conducted building-resolving numerical simulations of airflows in a densely built district of Osaka during the landfall of Typhoon Jebi (2018) and estimated the maximum instantaneous winds at a surface level being $50\text{--}60 \text{ m s}^{-1}$, comparable to the winds at a boundary-layer top. Takemi et al. (2019) emphasized that the variability of building heights in the densely built district makes surface-level strong winds severer. Thus, a geometrical feature of urban areas is considered to be critical in characterizing the strong wind hazards. However, in the study of Takemi et al. (2019), how the building density affects the gust appearances was not quantified.

Therefore, one of the purposes of this study is, by extending the work of Takemi et al. (2019), to further investigate the strong wind hazards in urban districts by performing large-eddy simulations (LESs). Different from the study of Takemi et al. (2019), the urban area of Kyoto City is chosen here, and the wind condition under Typhoon Jebi (2018) is assumed in the LES. Since there are a large number of historical buildings in Kyoto, assessing the strong wind hazards is an important task. In this sense, the LES model has an advantage in simulating airflows in urban areas because the model can explicitly represent unsteady, turbulent fluctuations of winds within a cluster of buildings in urban areas. In the previous study by Yoshida et al. (2018), they have performed LESs of airflows over Kyoto City, and the dataset is useful in demonstrating the gust characteristics. Thus, another focus of this study is placed on the instantaneous gust characteristics by using the data of Yoshida et al. (2018). In comparison with the LESs of Yoshida et al. (2018), additional experiments employing idealized building arrays are performed to examine whether the height-variability and arrangement of buildings have an impact on airflows in the urban area. By using the LES model, we will firstly explore the influences of building-height variability on airflows in urban-like, idealized building distributions, and secondly estimate the instantaneous winds within a real urban canopy of Kyoto City in order to gain insights into strong wind hazards in urban areas.

This paper firstly presents the morphological characteristics of Kyoto City by comparing those of Tokyo and Osaka in Section 2. Section 3 describes the LES model used in this study and the design of numerical experiments. Section 4 examines how building arrangements affect strong winds within idealized urban areas, and investigate strong wind characteristics in a business district of Kyoto in the case of Typhoon Jebi (2018). Section 5 summarizes the present study.

2. Morphology of Urban Areas in Japan: Kyoto, Osaka, and Tokyo

The geometrical characteristics of urban areas are described in terms of the spatial distributions of man-made buildings and structures. Ratti et al. (2002) derived urban morphological information by using fine-scale digital elevation model (DEM) datasets. According to Ratti et al. (2002), this study examines the urban morphological feature of Kyoto City. Kyoto is a historic city with a large number of temples, shrines, and old architectures and houses, some of which are recognized as World Heritage Site. At the same time, modern buildings and structures have been built over the decades. Thus, the city center hosts a mixture of historical and modern buildings. The morphological features of Kyoto City are examined with the use of high-resolution building data and are compared with those of other major cities in Japan: Osaka and Tokyo.

In order to derive the urban morphology, this study used the digital surface model (DSM) at the horizontal resolution of 2 m, provided by Kokusai Kogyo Co., Ltd. The original Level-1 DSM data were obtained by air-borne laser measurements, and were processed at the 2-m grid spacing as Level-2 data which we used here. Fig. 1a, b, and c show the spatial distribution of the buildings and their heights for Kyoto, Osaka, and Tokyo, respectively. Note that the ground elevation is excluded in the building height. In order to derive and compare the morphological characteristics for the three cities, the analysis area was centered on the business and densely built districts with the same size of the area as 2.2 km by 3.2 km. Fig. 1d, e, and f demonstrate the analysis areas for the three

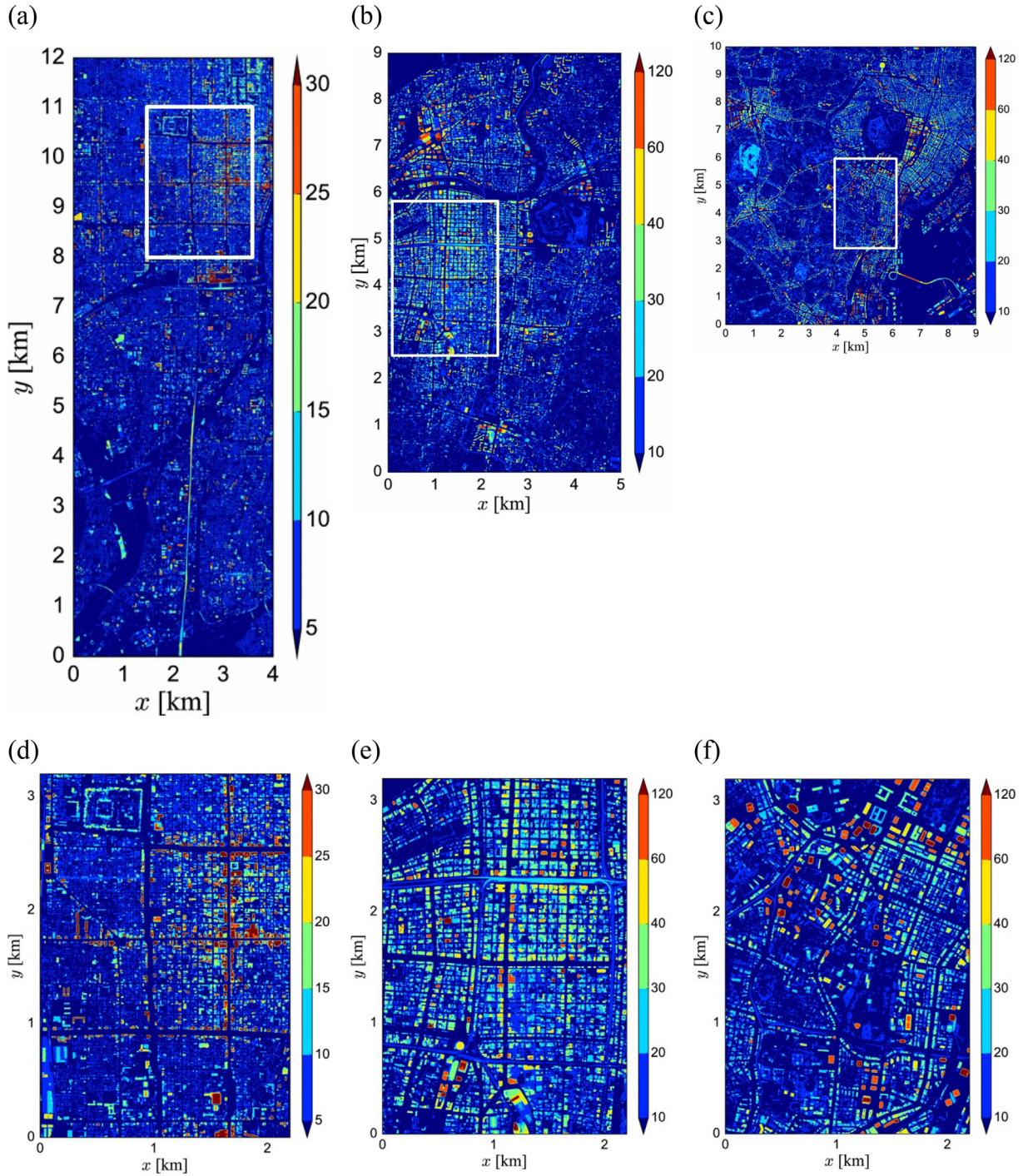


Fig. 1. The building height distributions of (a) Kyoto, (b) Osaka, and (c) Tokyo, with the height legends shown on the right of each panel. A 2.2 km by 3.2 km area indicated as the white box in each panel is enlarged in (d) Kyoto, (e) Osaka, and (f) Tokyo for the analysis of the morphological information.

cities.

The urban morphology is quantitatively characterized in terms of some of the roughness parameters examined in Ratti et al. (2002) and those used in Nakayama et al. (2011). The parameters examined here are average building height H_{ave} , the maximum building height H_{max} , standard deviation of building height σ_H , normalized building height variability V_H ($= \sigma_H/H_{ave}$), building plane area index λ_p , and building frontal area index λ_f . The plane area index is defined as the ratio of the total area occupied by buildings to

Table 1

Roughness parameters for the central districts of Kyoto, Osaka, and Tokyo.

| | H_{ave} (m) | H_{max} (m) | σ_H (m) | V_H | λ_p | λ_f |
|-------|---------------|---------------|----------------|-------|-------------|-------------|
| Kyoto | 11.6 | 56.6 | 7.8 | 0.67 | 0.46 | 0.29 |
| Osaka | 20.5 | 189 | 15.3 | 0.74 | 0.49 | 0.66 |
| Tokyo | 20.3 | 283 | 21.6 | 1.05 | 0.53 | 0.45 |

the total surface area, while the frontal area index is defined as the ratio of the total frontal area of buildings to the total surface area. If the obstacle height is uniform, MacDonald et al. (1998) theoretically obtained the analytical solution for roughness length z_0 as follows:

$$\frac{z_0}{H} = \left(1 - \frac{d}{H}\right) \exp\left[-\left(0.5 \frac{C_D}{\kappa} \left(1 - \frac{d}{H}\right) \lambda_f\right)^{-0.5}\right],$$

where H is the constant obstacle height, d is zero-plane displacement, C_D is drag coefficient, and κ is von Karman constant. This theoretical equation is able to reproduce the variation of roughness length in response to frontal area index. With the increase in building height variability, the theoretical equation of MacDonald et al. (1998) is no longer valid, and hence the effects of building height variability should be incorporated (Nakayama et al., 2011).

The above parameters were computed in the areas shown in Fig. 1d, e, and f. Table 1 summarizes the roughness characteristics of the urban surfaces of Kyoto, Osaka, and Tokyo. The building heights in Kyoto are overall lower than those in Osaka and Tokyo in terms of both the average and the maximum. In contrast, the building height variability which is normalized by the average height indicates that the height variability of Kyoto is comparable to that of Osaka and is much higher than the values of cities in Europe (i.e., London, Toulouse, and Berlin) (Ratti et al., 2002). In addition, the district of Kyoto is densely built, similar to the areas of Osaka and Tokyo. Such densely built environments of the three Japanese cities are similarly found in London and Toulouse (Ratti et al., 2002). However, the frontal area index of Kyoto is smaller than the values of Osaka and Tokyo, because of the lower building heights in Kyoto.

Fig. 2 shows the frequency distribution of the building heights in the central districts depicted in Fig. 1d, e, and f for Kyoto, Osaka, and Tokyo, respectively. About 60 to 70% of the total buildings in each district are lower than the averages, and about 25 to 35% of the total buildings have heights ranging from 1 to 2.5 times the average height. The distributions of the three cities up to the height of $2.5H_{ave}$ look similar among the three cities. However, the frequency of Kyoto has a local peak in the range of $2.5 - 3H_{ave}$, different from the feature of Osaka and Tokyo. Further increase in the height range demonstrates different behavior in the frequency distribution for the three cities. This means that the building plane area index evaluated at each height level has different features depending on the cities. Considering that the flow regime depends on the building plane area index (MacDonald et al., 1998) and that the plane area index can be estimated at each height level (Nakayama et al., 2011), the building height distributions will have different impact on airflows in each city.

From these analyses, the urban surface of the central district of Kyoto is characterized as having a building-height variability that is smaller than the cases of Osaka and Tokyo but much higher than those of the European cities examined in Ratti et al. (2002), and a high density of built areas, comparable to the densities of Osaka, Tokyo, and the European cities. The densely built environment with highly variable building heights is a common characteristic to the three Japanese cities.

3. LES model and experimental design

3.1. LES model

We use the LES model of Yoshida et al. (2018), which was originally developed by Nakayama et al. (2011) for simulating airflows

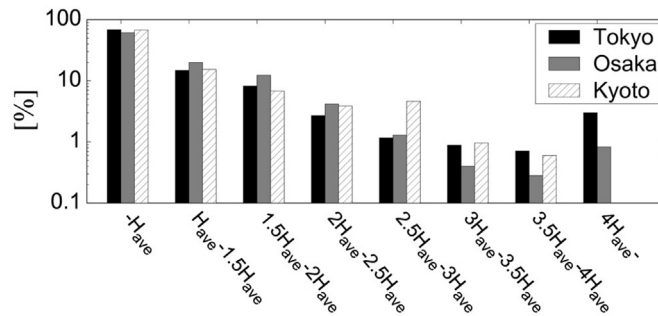


Fig. 2. The frequency distribution of building heights in the central districts of Kyoto, Osaka, and Tokyo. The heights are normalized by the average building height (H_{ave}) in each district.

over idealized arrays of urban-like roughness obstacles. The governing equations consist of the Navier-Stokes equation and the mass continuity equation with a spatial filter applied. An incompressible fluid without density stratification is assumed, because we focus on the neutral stability conditions. With the spatial filtering, the turbulence stress term appears in the Navier-Stokes equation, and the stress term is represented with a standard Smagorinsky model. The equation set is discretized on staggered grids in the Cartesian coordinate. The solid body is represented as an external forcing and is added as a body force in the Navier-Stokes equation. Within the Cartesian coordinate, each grid is characterized as a solid or a fluid cell. If a cell corresponds to a solid cell (i.e., within roughness obstacles), the additional forcing term is applied to the Navier-Stokes equation. This external body force is represented by the feedback forcing of Goldstein et al. (1993). The advantage of the LES model originally developed by Nakayama et al. (2011) is that the model can be easily implemented to simulating airflows over actual urban areas by representing the effects of roughness obstacles as the feedback forcing of Goldstein et al. (1993). Because the buildings in actual urban areas are distributed in a disorganized way such that the density, height, and arrangement of buildings is highly complex, flexibility in incorporating the actual buildings in the model is important. In the Cartesian coordinate system, separating fluid and solid grids is easily conducted with the use of digital elevation model (DEM) datasets which include individual buildings and structures. After separating the fluid and solid grids in the whole coordinate system, the external forcing term of Goldstein et al. (1993) is added to the momentum equations for the solid grids.

There are some parameters that should be specified in the LES model. Yoshida et al. (2018) conducted test experiments with the Smagorinsky constant C_s varied and compared the simulated results with the turbulence observations at the Ujigawa Open Laboratory located in the south of Kyoto City to find that the case with $C_s = 0.14$ best fitted to the observations. Thus, in this study the Smagorinsky constant was set to be 0.14. The external forcing term of Goldstein et al. (1993) includes three parameters, which were defined here in the same way as in Nakayama et al. (2011).

The validity of the present LES model has been confirmed through a wide range of applications to simulating turbulent flows over a business district of Tokyo during the landfall of a typhoon (Nakayama et al., 2012), airflows around the Fukushima Daiichi Nuclear Power Plant after the devastating earthquake and tsunami on 11 March 2011 (Nakayama et al., 2015), and turbulent flows and dispersion in Oklahoma City (Nakayama et al., 2016). A parallelization capability with Message Passing Interface (MPI) was implemented by Vanderbauwheide and Takemi (2015), enabling very-high-resolution simulations over a wide computational domain. The present LES model has been also validated with the observations at the Ujigawa Open Laboratory in Kyoto City (Yoshida et al., 2018).

The height and arrangement of buildings and structures in Kyoto City are obtained from the DSM dataset of Kokusai Kogyo Co., Ltd., which is shown in Fig. 1a. The dataset for Kyoto City is used as the lower boundary of the main computational domain. In order to provide turbulent inflows at the inlet of the main computational domain, we use the same approach as in Yoshida et al. (2018) by employing an additional computational domain to generate turbulent flows.

As in Yoshida and Takemi (2018) and Yoshida et al. (2018), we set two computational domains: one was a main computational domain; while the other was a driver domain to generate and accelerate turbulent inflows for the main computation domain. The idealized arrays of roughness obstacles were placed in the driver domain. The turbulent generation method in the driver domain was exactly the same as used in Yoshida et al. (2018). The details of the arrangement of the roughness obstacles placed in the driver domain were explained in Yoshida et al. (2018), and a uniform flow with a wind speed of 5 m s^{-1} is imposed at the inlet of the driver domain. Within the fetch of the driver domain with the roughness obstacles placed at the domain bottom in an idealized way, turbulent flows were generated. The turbulent properties of the inflows generated in the driver domain were given in the supplementary material of Yoshida et al. (2018).

The turbulent inflows generated with this procedure were imposed at the inlet of the main computational domains in all the numerical experiments as described in the following subsections. In the idealized experiments the idealized roughness arrays were used, while in the experiments for flows over the actual urban area the real building dataset was used to set the lower boundary geometry. The numerical experimental settings are described in the following subsections.

3.2. Experimental design: Idealized experiments

In this study, we used the LES outputs of Yoshida et al. (2018) who conducted LESs of airflows over Kyoto City. In addition, we conducted numerical experiments on airflows over urban-like, idealized building arrays in order to demonstrate the effects of building-height variability and building arrangement.

The arrangements of the roughness obstacles for the present idealized numerical experiments are shown in Fig. 3. Two numerical experiments were conducted. The one is SQ in which a square array of obstacles with the height of 10.3 m is placed at the lower boundary. The other is VAR in which two types of obstacles with different height are placed in a staggered way as shown in Fig. 3. The height of the lower obstacle H_{low} is 6.5 m, and that of the higher obstacle H_{high} is 21.7 m, which are intended to keep the mean height of the building arrangement in VAR being 10.3 m. The building plane area index in both SQ and VAR was assumed to be the same value of 0.29, which corresponds to the plane area index evaluated in the computational domain of 11 km by 2 km used in Yoshida et al. (2018). The two numerical experiments were compared with the two simulations CTL and UNI conducted in Yoshida et al. (2018). In CTL the actual building distributions and heights were used, while in UNI all the buildings were imposed to have the same height of 10.3 m.

The computational area covered by the sensitivity experiments of VAR and SQ, as indicated in Fig. 3, is 11 km by 2 km; this area size is the same as was used in Yoshida et al. (2018) for simulating airflows over Kyoto City. As in Yoshida et al. (2018), the time step was set to be 0.05 s, and the horizontal grid spacing was 4 m. The Courant number was about 0.0625. The integrated time period was 120 min, and the simulated outputs for the last 30 min were used for the present analysis. Therefore, the total cost of the simulations

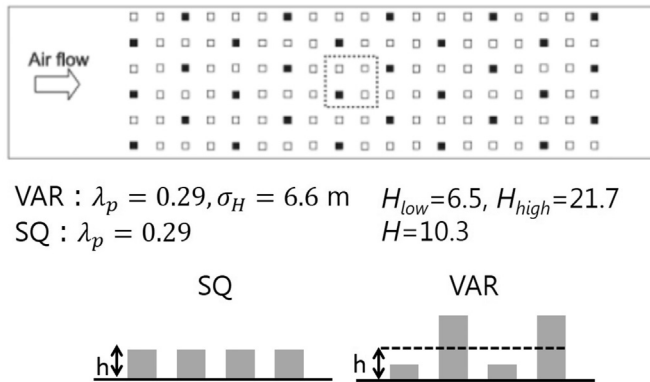


Fig. 3. The arrangement of the roughness obstacles used in the numerical experiments SQ and VAR. See the main text for the details of SQ and VAR.

for the idealized roughness distribution was actually the same with that for the actual urban case of Kyoto City. These settings were chosen because the comparisons between the actual urban cases and the idealized urban-like roughness cases are done in a more straightforward way.

3.3. Experimental design: Case of a typhoon landfall

Strong wind hazards in Kyoto City are investigated here, as a case analysis for Typhoon Jebi (2018). This typhoon spawned severe winds along its track. Fig. 4 exhibits the mean and maximum instantaneous wind speeds observed at the meteorological observation station in Kyoto City, operated by Japan Meteorological Agency, and the atmospheric environmental monitoring site installed on the top of Kyoto Tower, operated by the local government office of Kyoto City. The anemometer heights of the meteorological station and the atmospheric environmental monitoring site are 17.6 m and 121 m, respectively. At the meteorological station, the maximum instantaneous wind speed during the passage of Typhoon Jebi was 39.4 m s^{-1} , which is the second highest record since the station started to record the maximum instantaneous wind in September 1881. Note that the highest record at the Kyoto meteorological station is 42.1 m s^{-1} , resulting from Muroto Typhoon in 1934 (which recorded the minimum surface pressure of 911.6 hPa at the meteorological station in Muroto). On the other hand, the maximum instantaneous wind speed at Kyoto Tower was 57.6 m s^{-1} . It is interesting to mention here that the gust factor, defined as the ratio of the maximum instantaneous wind speed to the mean wind speed, is generally larger at the meteorological station than at the environmental monitoring site; the mean gust factor averaged during the time period shown in Fig. 4 is 1.33 at the environmental monitoring site while is 2.04 at the meteorological station.

A challenge here is whether the LES model can reproduce such a wind variability. Fig. 5 demonstrates the computational area used for the present LES, including Kyoto Station Building, Kyoto Tower, and the surrounding business districts as well as some historical temples and architectures. Roughness parameters for this computational area are as follows: $\lambda_p = 0.36$, $\lambda_f = 0.25$, $H_{ave} = 11.8$ (m), and $\sigma_H = 8.9$ (m). The computational settings are the same as those used in Takemi et al. (2019), except for the analysis area. The turbulent inflows generated in a driver domain were ingested at the southern boundary (the left boundary in Fig. 5) as the southerly wind, because the southerly wind was the dominant wind direction during the strong wind period in Kyoto City associated with the typhoon passage.

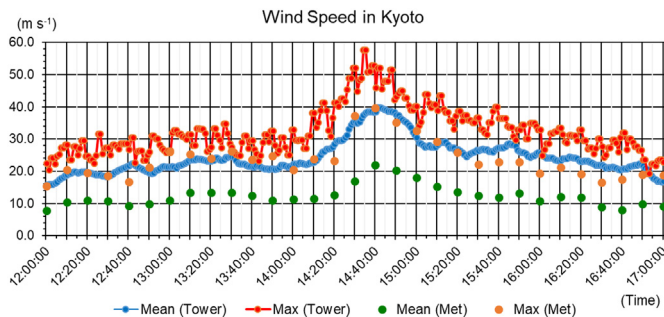


Fig. 4. Time series of wind speeds in Kyoto City in the afternoon of 4 September 2018. Shown are the mean wind speeds observed at the meteorological station (green dot) and at the Kyoto Tower atmospheric environmental monitoring site (blue dot and line) and the maximum instantaneous wind speeds at the meteorological station (orange dot) and at the Kyoto Tower site (red dot and line). The time intervals of the data at the meteorological station and at the Kyoto Tower site are 10 min and 1 min, respectively. (For interpretation of the references to colour in this figure legend, the reader is referred to the web version of this article.)

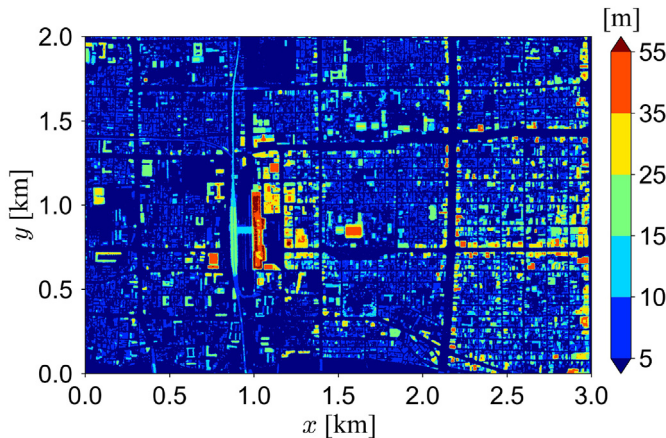


Fig. 5. The building height distribution in the area of 3 km (x axis, from south to north) and 2 km (y axis, from west to east) in Kyoto. The highest building located at around $x = 1$ km and $y = 1$ km is Kyoto Station Building.

4. Analysis of strong wind hazards in an urban area

4.1. Mapping wind environment

By using the LES outputs of Yoshida et al. (2018), we are able to assess the impacts of strong winds on local-scale environment and hazard in urban areas. Fig. 6 demonstrates maps of flow characteristics in the business district of Kyoto. The maximum wind speed at the height of $0.5H_{ave}$ is obtained from the maximum value at each grid point during the simulated time period. As expected, strong winds occur along wide streets and in open spaces (Fig. 6a). If this maximum wind speed is normalized by the mean wind speed at the boundary-layer top (as defined in Ahmad et al., 2017), this ratio is also larger along the wide streets and in open spaces than within the densely built areas (Fig. 6b). The gust factor, defined as the ratio of the maximum to the mean wind speed at a local point, appears quite differently from the spatial pattern of the maximum winds. Because the mean winds within densely built areas or behind massive buildings or behind a cluster of buildings are generally weak, gust factors there become large with strong instantaneous winds. Thus, the features seen in Fig. 6 emphasize that maximum winds will be stronger along major streets and in open spaces while instantaneous gusts will be more enhanced within densely built areas.

Fig. 7 shows and compares the horizontal distributions of Reynolds stress, normalized by the squared mean wind speed at the top of the boundary layer, at the height of $2.5H_{ave}$ for the cases examined in Yoshida et al. (2018) (i.e., CTL and UNI) and the cases examined here (i.e., SQ and VAR). A sharp contrast and large magnitudes are seen around the high-rise buildings above $2.5H_{ave}$ in CTL (Fig. 7a). In the upper-middle part of Fig. 7a, there are high-rise building clusters including Kyoto Station, which produce a large magnitude of Reynolds stress in CTL. In contrast, such a large magnitude of Reynolds stress is never seen in UNI (Fig. 7b). Because both CTL and UNI use the same building arrangement, the difference is due to the influences from the building-height variability in the corresponding district. This was described more in detail in Yoshida et al. (2018).

If the idealized arrangement was used, the pattern seen in UNI is basically unchanged, but the magnitude overall reduced in SQ (Fig. 7c). Note that the difference between UNI and SQ is whether the actual spatial distribution of buildings is employed. Thus, the results shown in Fig. 7b and c suggest that the arrangement of buildings does not have significant impacts on overall turbulent statistics, when the obstacle height is uniform. With the height variability of the roughness obstacles added (i.e., the VAR case), the Reynolds stress becomes more enhanced than in the SQ case. The clear difference between VAR and SQ indicates that the building-height variability is more influential in characterizing the turbulent characteristics than the arrangement of buildings. The contrast of major and minor Reynolds stress represented in VAR is basically observed in the actual case of CTL. In addition, the comparison between the results of CTL and VAR suggests that the complicated distribution of the buildings in actual urban areas further strengthens the magnitude of the Reynolds stress. For example, a large magnitude of Reynolds stress seen within the high-rise building clusters around Kyoto Station in CTL is not seen in VAR.

The vertical profiles of the mean streamwise wind, the Reynolds stress, and the dispersive flux are demonstrated in Fig. 8. Compared with the mean winds in UNI and SQ, those in CTL and VAR are significantly reduced not only within the urban canopy layer (below the level of the mean building height H_{ave}) but also above the layer up to the level of 20 times H_{ave} . Decreased mean winds are more enhanced at around the height of H_{ave} in VAR than in CTL. This difference in mean winds between CTL and VAR is considered to be due to enhanced vertical momentum exchanges more in CTL (where building height varies in a realistic and complicated way) than in VAR (where building height varies regularly). Actually, there are regions of large magnitudes of Reynolds stress around the high-rise building clusters in CTL, which has significant impacts on overall vertical momentum exchanges not only in the nearby area around Kyoto Station but also in the whole analysis domain. Because of the enhanced momentum exchanges, the mean winds at around the height of H_{ave} in CTL are less reduced than in VAR.

The Reynolds stress below H_{ave} is more enhanced in CTL and UNI than in SQ and VAR, while the stress above H_{ave} rapidly

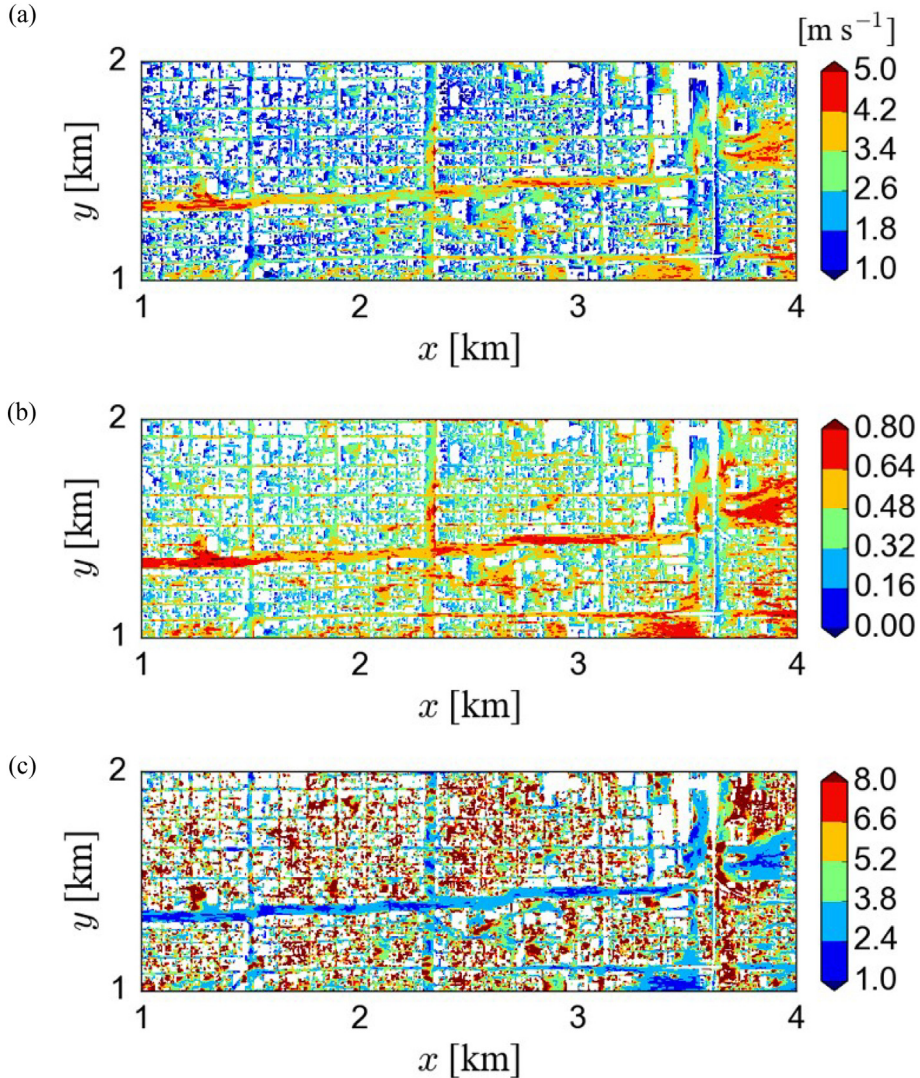


Fig. 6. The spatial distribution of (a) the maximum wind speed at $z = 0.5H_{ave}$, (b) the maximum wind speed at $z = 0.5H_{ave}$ divided by the mean wind speed at the boundary-layer top, and (c) the gust factor $z = 0.5H_{ave}$ (the maximum wind speed divided by the mean wind speed) in the business district of Kyoto.

increases and becomes larger in VAR than in the other cases (Fig. 8b). The enhanced nature of the Reynolds stress below the mean building height in CTL and UNI is due to the irregularity in the building arrangement of the actual urban area. The peaks of the Reynolds stress at the levels of $2\text{--}5H_{ave}$ in CTL and VAR are considered to be due to the effects of the building height variability. Especially, the most significant peak seen in VAR among all the cases appears at the height slightly above H_{high} , i.e., 21.7 m. This suggests that the higher building significantly controls the magnitude of the Reynolds stress. The comparison between CTL and VAR also indicates that the high-rise building clusters around Kyoto Station in CTL, even though their area size is limited, have significant impacts on the domain-averaged Reynolds stress fields at the extended height levels ranging from about $2H_{ave}$ to $10H_{ave}$ and higher. As demonstrated in Park et al. (2015) and Han et al. (2017), the impacts of high-rise building clusters on turbulent exchanges are significant not only locally but also globally.

On the other hand, the dispersive flux below H_{ave} is significantly larger in UNI and SQ than in CTL and VAR (Fig. 8c). Because the dispersive flux is determined from the contribution of temporally averaged flows, the cases with the uniform building height (UNI and SQ), in which components of mean flows are larger than in the cases with variable building height (CTL and VAR), indicate larger dispersive flux especially within the canopy layer. The roughness density λ_p was 0.29 in all the experimental cases; this value is within the range indicating a regime of wake interference flow over urban buildings with uniform height (Oke, 1988). However, the increase in the variability of building height results in unsteadiness of flow patterns within urban canopies (Nakayama et al., 2011). Therefore, the cases with uniform building height will exhibit steady airflow patterns more frequently than the cases with variable building height. This difference leads to the different representations of dispersive flux in the urban canopy as shown in Fig. 8c. In

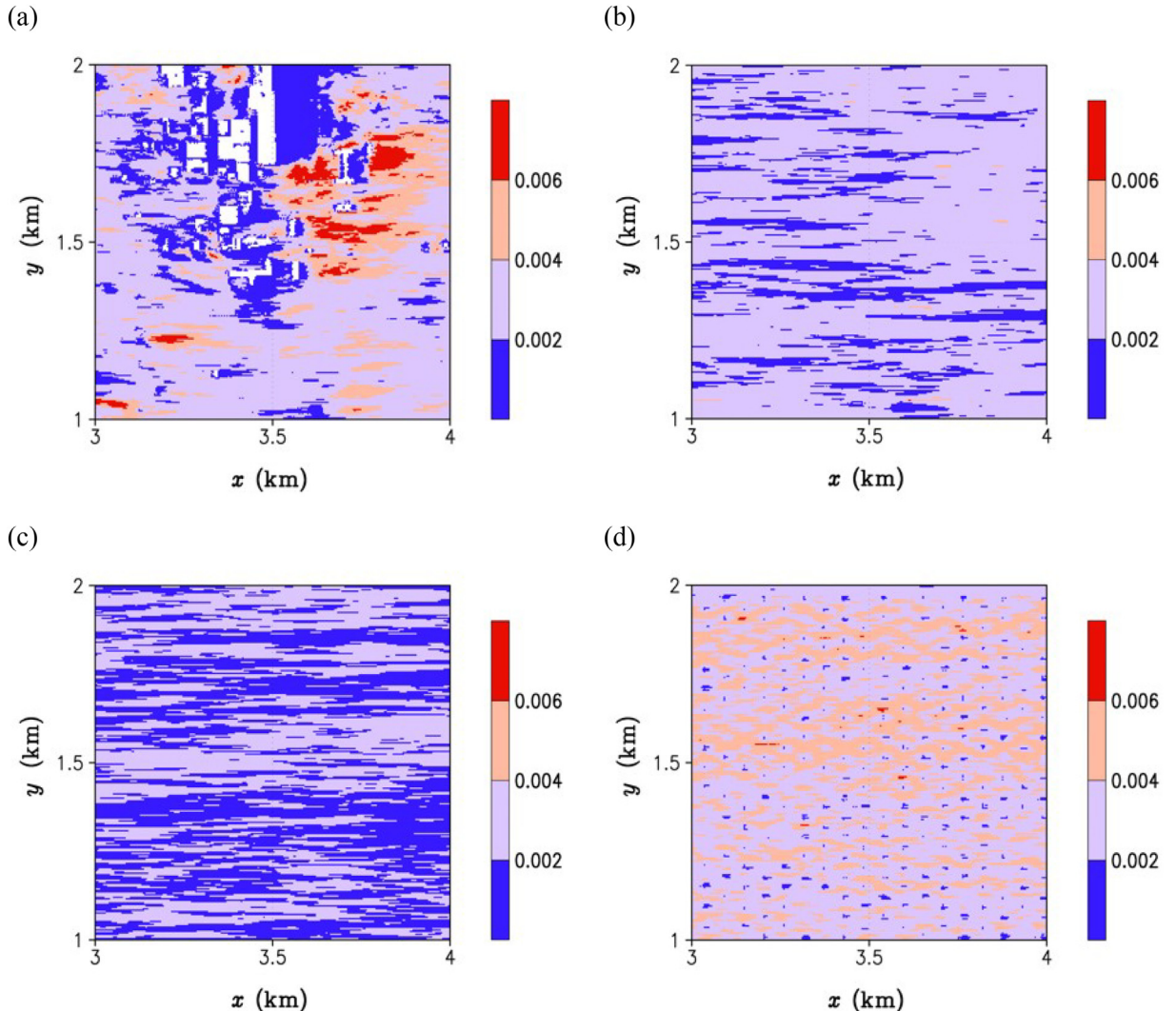


Fig. 7. The horizontal distribution of Reynolds stress, normalized by the upper-level mean wind squared, at the height of $2.5H_{ave}$ for (a) CTL, (b) UNI, (c) SQ, and (d) VAR.

other words, irregular and anomalous winds are considered to be evident in areas with a complex building arrangement, as seen in the actual urban areas.

From the results shown in this subsection, it is suggested that instantaneous winds are larger in the case with building-height variability (VAR) than in the case with constant building height (SQ) and are further enhanced in the case with the actual, complex building arrangement (CTL) than in the case with the regular building arrangement (VAR). Thus, the actual urban area with complex building arrangement and building-height variability is potentially hazardous for the occurrence of strong winds. Therefore, the characteristics of extreme winds will be examined in the next subsection.

4.2. A case analysis of strong winds by an extreme typhoon

In this subsection, the results from the real-case simulations for the case of Kyoto City are presented.

Fig. 9 compares the times series of the observed and simulated instantaneous wind speeds for the time period from 14:20 to 14:50 Japan Standard Time (JST) 4 September 2018. Wind speeds are normalized by the mean wind speed (\bar{U}) at the simulated boundary-layer top (i.e., 326 m) averaged over the analysis area and the simulated time period. Note that the observed winds are available at the 1-min interval and are the maximum instantaneous value during each 1-min interval, while the simulated outputs are available at the 1-s interval. The maximum envelop from the simulation seems to well capture the observed maximum instantaneous values. The mean gust factor for the 30-min period from the observation is 1.35, while the simulated gust factor averaged for the time period is 1.40; the present LES is able to reproduce the gustiness at the Kyoto Tower site.

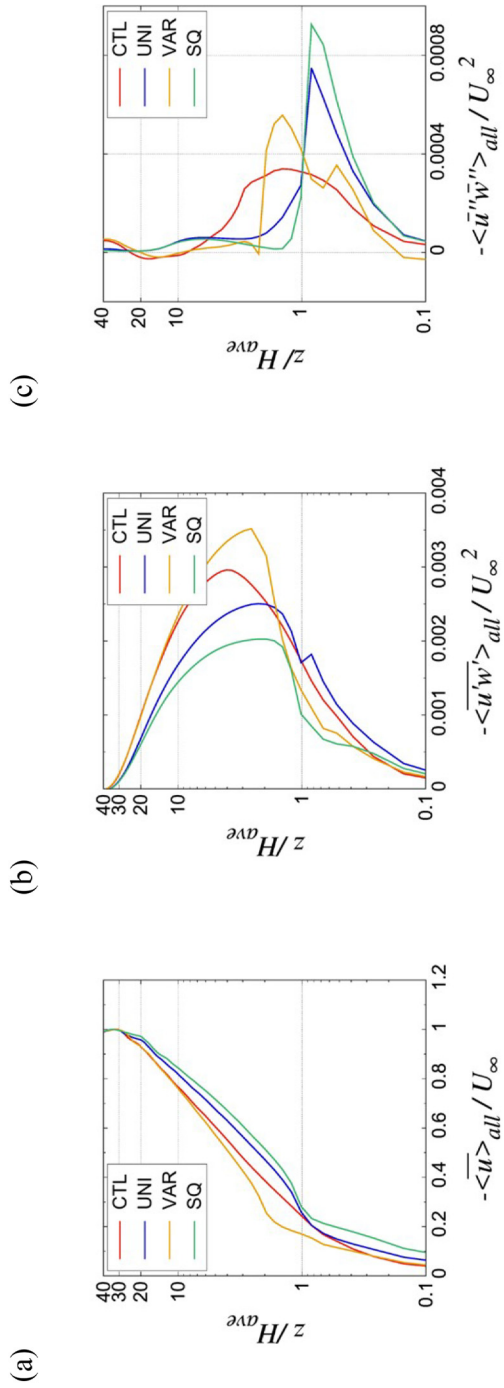


Fig. 8. The vertical profiles of (a) the mean streamwise wind, (b) the Reynolds stress, and (c) the dispersive flux for CTL, UNI, SQ, and VAR. The values are normalized in terms of the mean wind at the boundary-layer top. The height on the vertical axis is normalized by the mean building height H_{ave} .

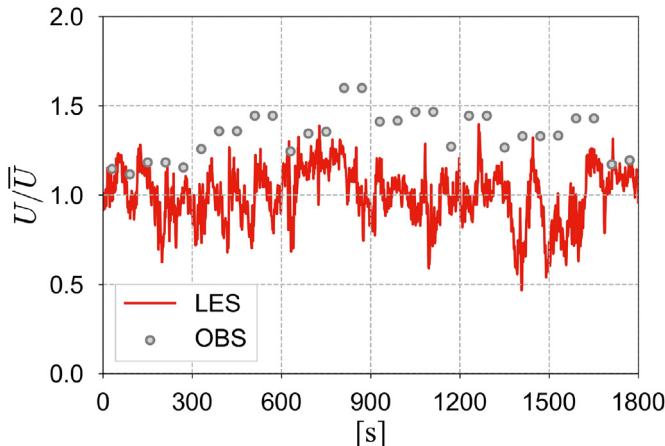


Fig. 9. Time series of wind speeds observed at the Kyoto Tower site (gray circle) and simulated by the LES model at the point corresponding to the Kyoto Tower site (red line) for 30 min corresponding to the period from 14:20 to 14:50 JST 4 September 2018. The observed maximum instantaneous wind speed during 1-min interval is normalized by the observed mean wind for the 30-min period, while the simulated instantaneous wind speed is normalized by the simulated mean wind for the 30-min period. (For interpretation of the references to colour in this figure legend, the reader is referred to the web version of this article.)

Based on the favorable performance of the present LES, an analysis on the strong wind hazard in the urban area of Kyoto City is made. Fig. 10 shows the temporal mean and the maximum wind speeds (normalized by the mean wind speed \bar{U}) at the height of $0.5H_{ave}$ during the simulated time period in the analysis area. The wind speeds shown here are normalized by \bar{U} . In Fig. 10a, it is seen that the mean winds are stronger along south-north-oriented major streets and in some open spaces. In contrast, the wind speeds are overall very weak around the building clusters of Kyoto Station. This is due to the deceleration of winds within the urban canopy by blockage from densely built, high-rise buildings. On the other hand, the maximum winds demonstrate some contrasting signatures (Fig. 10b). Similar to the features found in the mean winds, the maximum winds become stronger along south-north-oriented major streets and over open spaces. Different points from the features shown in Fig. 10a are that the maximum winds are significantly stronger around and within the building clusters of Kyoto Station and also along an east-west-oriented major streets at around $x = 2.1$ km. As seen in Fig. 5, these areas are characterized as having high-rise buildings embedded in wide-spread low-rise buildings or open spaces. Thus, the gustiness increases in areas with a mixture of high-rise and low-rise buildings. The wind speeds in those areas amount to the mean wind at the boundary-layer top (i.e., 326 m). Considering that the observed maximum wind speed at the height of 121 m at Kyoto Tower is 57.6 m s^{-1} , the maximum wind speed at the height of 326 m would be greater than 57.6 m s^{-1} . This suggests that the surface maximum winds reached 57.6 m s^{-1} or greater in some areas around Kyoto Station or along some major streets. Therefore, densely built areas with high-rise buildings have potentially a serious risk of being damaged by severe winds, which was found in the characteristics of gusty winds in an urban district of Osaka City (Takemi et al., 2019).

The characteristics of the surface wind gustiness are further examined in terms of building plane-area index (λ_p). The plane area index is computed as the total plane area covered by buildings and structures in a unit area of 500 m by 500 m within the computational domain indicated by Fig. 5. A reason why we chose the unit area size of 500 m by 500 m is that the downscaling experiments by mesoscale meteorological models are currently aiming at a horizontal grid spacing on the order of 100 m in order to gain benefits from the fine-scale representations of topography (Takemi, 2013; Takayabu et al., 2016; Takemi and Ito, 2020). From a convective-scale point of view, Bryan et al. (2003) indicated that the horizontal resolution having the order of 100 m is necessary to adequately resolve turbulent behaviors of convective motions. In addition, Takemi and Rotunno (2003) showed that spatial filtering in simulations with the grid spacing on the order of 1 km introduces unnatural grid-scale fluctuations in convective-scale motions. Actually, the grid spacing on the order of 1 km is regarded as a “terra incognita” zone (Wyngaard, 2004). Furthermore, Japan Meteorological Agency is targeting to develop a limited-area numerical model with the resolution on the order of 100 m, as a next-generation numerical weather forecasting model (personal communication). These considerations led us to decide the unit area having a 500-m size in this study. The choice of 500 m itself is arbitrary, and in our future studies we will explore the proper horizontal scale to define the roughness properties in various urban districts.

Fig. 11 indicates the relationship between surface maximum winds and plane area index. The surface winds are indicated in terms of the ratios against the mean wind at the boundary-layer top, and the ratios are computed for the surface winds at the height of $0.5H_{ave}$ and $1.0H_{ave}$ as a grid-point basis except the points within buildings and structures and are averaged over the grid points in each unit area. It is seen in Fig. 11 that the ratios generally increase with the decrease in λ_p . This tendency is consistent with that found in a case of Tokyo studied by Ahmad et al. (2017). In the analysis region of Kyoto City, the areas having higher λ_p values are characterized by densely built districts with mostly low-rise buildings, while the areas with lower λ_p values are by having high-rise buildings, open spaces, and major streets. Thus, the features seen in Fig. 10b are reflected on the tendency shown in Fig. 11.

According to Oke (1988), the λ_p value around 0.2–0.3, at which the ratios of the surface maximum winds are higher, falls within the range of wake interference flow. In this flow regime, flow fields in general indicate an unsteady, turbulent nature within the urban

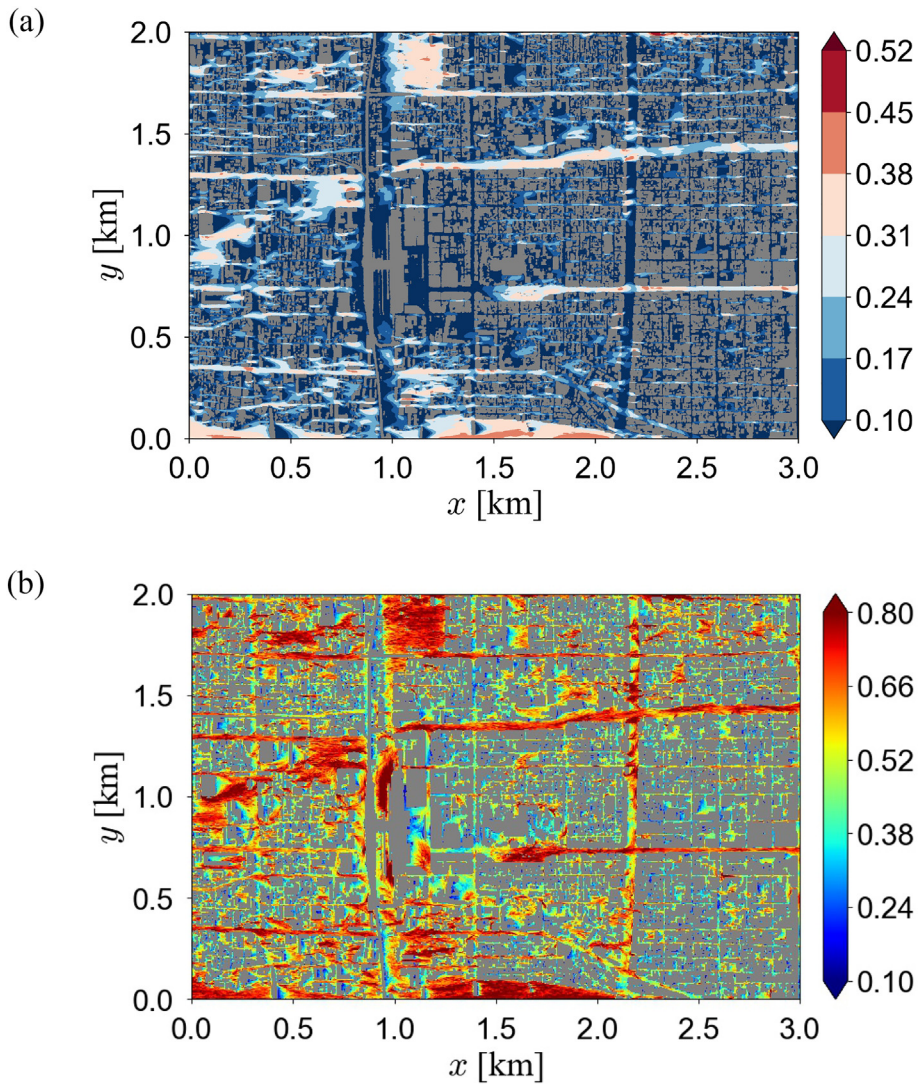


Fig. 10. (a) Mean and (b) maximum wind speeds at the height of $0.5H_{ave}$ (about 6 m) during the simulated time period of 30 min. The wind speeds are normalized by the mean wind at the boundary-layer top (\bar{U}), and the ratios of the wind speeds against \bar{U} are indicated.

canopy. The variability of building height will enhance such an unsteady nature (Nakayama et al., 2011; Yoshida and Takemi, 2018). The result shown in Fig. 11 suggests that wind gustiness clearly appears in a pronounced way especially in the regime of wake interference flow.

5. Summary and conclusions

This study investigated the characteristics of turbulent airflows and their instantaneous peaks and thereby demonstrated potential hazards due to strong winds in an urban area as a case study for Kyoto City by employing an LES modeling approach. The actual building data were used to simulate turbulent flows over a business district in Kyoto City. The analysis of morphology of urban areas of Kyoto City in comparison to those of Osaka and Tokyo indicated that the geometrical features of an urban district in Kyoto City is characterized as having a high variability of building heights and a high density of building areas than those found in cities in Europe (Ratti et al., 2002), similarly seen in the cases of Osaka and Tokyo.

By using the LES outputs of Yoshida et al. (2018) as well as conducting additional sensitivity experiments for flows over idealized roughness obstacles, we demonstrated that maximum instantaneous winds become stronger along major streets and in open spaces while gustiness is increased within densely built areas. The sensitivity experiments of airflows over regularly distributed roughness obstacles in addition to the simulations of airflows over the actual urban area of Kyoto City indicated that regular arrangements of buildings would enhance steady natures of airflows within urban canopy, and that the building height variability would increase unsteadiness of airflows. From the comparison of the LESs of airflows over the actual urban area (Yoshida et al., 2018) and over the

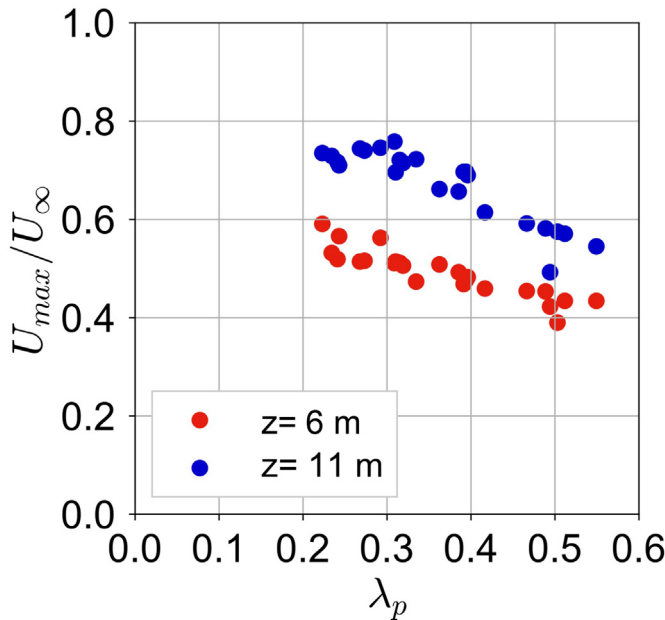


Fig. 11. The ratio of the surface maximum wind speed to the mean wind at the boundary-layer top against building plane-area index. The ratios for the surface maximum wind at the height of $0.5H_{ave}$ ($z = 6\text{ m}$) (red circle) and at the height of $1.0H_{ave}$ ($z = 11\text{ m}$) (blue circle) are indicated. (For interpretation of the references to colour in this figure legend, the reader is referred to the web version of this article.)

regularly distributed roughness obstacles, it is suggested that the actual, complex arrangement of buildings would further strengthen instantaneous winds in addition to the effect of the building height variability.

We further examined hazards induced by strong winds by assuming an actual condition of extreme winds. We chose Typhoon Jebi (2018) as a case. After confirming the validity of the present LES model against the observation at a high elevation equipped on Kyoto Tower, the LES results for surface winds showed that sustained winds are generally stronger along the major streets oriented in the streamwise direction and over open spaces while instantaneous winds become stronger especially within areas having high-rise buildings embedded in wide-spread low-rise buildings or open spaces. Such gustiness seen in the surface winds was examined in terms of building plane area index λ_p . The wind gustiness increases with the decrease in λ_p in the analysis region of Kyoto City. The peak values of the wind gustiness were found in the λ_p range showing a wake interference flow regime (Oke, 1988). As demonstrated in the present analyses on the data of Yoshida et al. (2018) and the sensitivity experiments, the building height variability enhances a turbulent nature of airflows in urban canopy, and the complex arrangement of actual buildings further strengthens instantaneous winds. Therefore, the present study concludes that both the building height variability and the actual complex building arrangement are considered to enhance the gustiness of surface winds. Such urban geometrical features should be taken into account in order to assess the urban hazards resulting from strong winds.

Demonstrating the use of the LES model for assessing the atmospheric environment and the natural hazards is an important scientific contribution of this study. For example, considering that a typhoon is one of the major natural hazards in Japan and also in East and Southeast Asia, assessing the impacts of hazards produced by typhoons is an important step for preventing and mitigating resulting disasters. Impacts of hazards will occur at local-scales, and therefore detailed information of hazards at local-scales is prerequisite. Especially in densely built urban districts, the impacts of hazards are quantitatively different depending on the specific districts in cities. We have indicated that the LES model can provide quantitative information of extreme winds in terms of the maximum instantaneous winds within urban districts.

There are common understanding of the importance and usefulness of dynamical downscaling techniques in assessing the impacts of extreme weather under future global warming (Takemi et al., 2016a). However, such downscaling experiments for impact assessment studies are conducted with the use of a mesoscale meteorological model, such as the WRF model, at the horizontal grid spacing of around 1 km. At this grid, the detailed structure of urban areas cannot be explicitly represented. By coupling a mesoscale meteorological model with an LES model, we will be able to simulate turbulent airflows in actual urban areas under real meteorological settings. Such a coupling would enable to investigate environmental hazard under various meteorological conditions.

Declaration of Competing Interest

All the authors declare that they have no competing interests.

Acknowledgments

The comments by two anonymous reviewers and the editor are greatly acknowledged in improving the original manuscript. This study was supported by Japan Society for Promotion of Sciences Kakenhi 18H01680, 18K19953, and the Environment Research and Technology Development Fund (2-1905) of the Environmental Restoration and Conservation Agency of Japan. Wim Vanderbauwheide was supported by UK EPSRC grant EP/L026201/1. The data observed at Kyoto Tower were provided by Environmental Policy Department, City of Kyoto.

References

- Ahmad, N.H., Inagaki, A., Kanda, M., Onodera, N., Aoki, T., 2017. Large-eddy simulation of the gust index in an urban area using lattice Boltzmann method. *Bound.-Layer Meteorol.* 163, 447–467.
- Alford, A.A., Biggerstaff, M.I., Carrie, G.D., Schroeder, J.L., Hirth, B.D., Waugh, S.M., 2019. Near-surface maximum winds during the landfall of Hurricane Harvey. *Geophys. Res. Lett.* 46, 973–982.
- Belcher, S.E., 2005. Mixing and transport in urban areas. *Phil. Trans. Roy. Soc. A* 363, 2947–2968.
- Bottema, M., 1997. Urban roughness modeling in relation to pollutant dispersion. *Atmos. Environ.* 31, 3059–3075.
- Bou-Zeid, E., Overney, J., Rogers, B.D., Parlange, M.B., 2009. The effects of building representation and clustering in large-eddy simulations of flows in urban canopies. *Bound.-Layer Meteorol.* 132, 415–436.
- Bryan, G.H., Wyngaard, J.C., Fritsch, J.M., 2003. Resolution requirements for the simulation of deep moist convection. *Mon. Weather Rev.* 131, 2394–2416.
- Castro, I.P., 2017. Are urban-canopy velocity profiles exponential? *Bound.-Layer Meteorol.* 164, 337–351.
- Cheng, H., Castro, I.P., 2002. Near wall flow over urban-like roughness. *Bound.-Layer Meteorol.* 104, 229–259.
- Fernando, H.J.S., 2010. Fluid dynamics of urban atmospheres in complex terrain. *Ann. Rev. Fluid Mech.* 42, 365–389.
- Fernando, H.J.S., Zajic, D., Di Sabatino, S., Dimitrova, R., Hedquist, B., Dallman, A., 2010. Flow, turbulence, and pollutant dispersion in urban atmospheres. *Phys. Fluids* 22, 051301.
- Giometto, M., Christen, A., Meneveau, C., Fang, J., Krafczyk, M., Parlange, M., 2016. Spatial characteristics of roughness sublayer mean flow and turbulence over a realistic urban surface. *Bound.-Layer Meteorol.* 160, 425–452.
- Goldstein, D., Handler, R., Sirovich, L., 1993. Modeling a noslip flow boundary with an external force field. *J. Comput. Phys.* 105, 354–366.
- Grimmond, C.S.B., Oke, T.R., 1999. Aerodynamic properties of urban areas derived from analysis of surface forms. *J. Appl. Meteorol.* 38, 1262–1292.
- Han, B.-S., Park, S.-B., Baik, J.-J., Park, J., Kwak, K.-H., 2017. Large-eddy simulation of vortex streets and pollutant dispersion behind high-rise buildings. *Quart. J. Roy. Meteorol. Soc.* 143, 2714–2726.
- Hertwig, D., Gough, H.L., Grimmond, S., Barlow, J.F., Kent, C.W., Lin, W.E., Robins, A.G., Hayden, P., 2019. Wake characteristics of tall buildings in a realistic urban canopy. *Bound.-Layer Meteorol.* 172, 239–270.
- Hill, K.A., Lackmann, G.M., 2011. The impact of future climate change on TC intensity and structure: a downscaling approach. *J. Clim.* 24, 4644–4661.
- Hunter, L.J., Watson, I.D., Johnson, G.T., 1990. Modelling air flow regimes in urban canyons. *Energy Build.* 15, 315–324.
- Hussain, M., Lee, B.E., 1980. A wind tunnel study of the mean pressure forces acting on large groups of low-rise buildings. *J. Wind Eng. Ind. Aerodyn.* 6, 207–225.
- Ito, R., Takemi, T., Arakawa, O., 2016. A possible reduction in the severity of typhoon wind in the northern part of Japan under global warming: a case study. *SOLA* 12, 100–105. <https://doi.org/10.2151/sola.2016-023>.
- Kanada, S., Takemi, T., Kato, M., Yamasaki, S., Fudeyasu, H., Tsuboki, K., Arakawa, O., Takayabu, I., 2017a. A multi-model intercomparison of an intense typhoon in future warmer climates by four 5-km-mesh models. *J. Clim.* 30, 6017–6036.
- Kanada, S., Tsuboki, K., Aiki, H., Tsujino, S., Takayabu, I., 2017. Future enhancement of heavy rainfall events associated with a typhoon in the midlatitude regions. *SOLA* 13, 246–251. <https://doi.org/10.2151/sola.2017-045>.
- Kanda, M., 2006. Large-eddy simulations on the effects of surface geometry of building arrays on turbulent organized structures. *Bound.-Layer Meteorol.* 118, 151–168.
- Kanda, M., Inagaki, A., Miyamoto, T., Gryschka, M., Raasch, S., 2013. A new aerodynamic parametrization for real urban surfaces. *Bound.-Layer Meteorol.* 148, 357–377.
- Kato, N., Ohkuma, T., Kim, J.R., Marukawa, H., Niihori, Y., 1992. Full scale measurements of wind velocity in two urban areas using an ultrasonic anemometer. *J. Wind Eng. Ind. Aerodyn.* 41, 67–78.
- Knight, R.I., Khalid, F., 2015. Evaluation of the potential of friction surface analysis in modelling hurricane wind damage in an urban environment. *Nat. Hazards* 76, 891–911.
- Lackmann, G.M., 2015. Hurricane Sandy before 1900 and after 2100. *Bull. Am. Meteorol. Soc.* 96, 547–560. <https://doi.org/10.1175/BAMS-D-14-00123.1>.
- Li, H., Cui, G., Zhang, Z., 2018. A new scheme for the simulation of microscale flow and dispersion in urban areas by coupling large-eddy simulation with mesoscale models. *Bound.-Layer Meteorol.* 167, 145–170.
- MacDonald, R.W., Griffiths, R.F., Hall, D.J., 1998. An improved method for the estimation of surface roughness of obstacle arrays. *Atmos. Environ.* 32, 1857–1864.
- Nakayama, H., Takemi, T., Nagai, H., 2011. LES analysis of the aerodynamic surface properties for turbulent flows over building arrays with various geometries. *J. Appl. Meteorol. Climatol.* 50, 1692–1712.
- Nakayama, H., Takemi, T., Nagai, H., 2012. Large-eddy simulation of urban boundary-layer flows by generating turbulent inflows from mesoscale meteorological simulations. *Atmos. Sci. Lett.* 13, 180–186. <https://doi.org/10.1002/asl.377>.
- Nakayama, H., Takemi, T., Nagai, H., 2015. Large-eddy simulation of turbulent winds during the Fukushima Daiichi Nuclear Power Plant accident by coupling with a meso-scale meteorological simulation model. *Adv. Sci. Res.* 12, 127–133. <https://doi.org/10.5194/asr-12-127-2015>.
- Nakayama, H., Takemi, T., Nagai, H., 2016. Development of local-scale high-resolution atmospheric dispersion model using large-eddy simulation. Part 5: Detailed simulation of turbulent flows and plume dispersion in an actual urban area under real meteorological conditions. *J. Nuclear Sci. Tech.* 53, 887–908. <https://doi.org/10.1080/00223131.2015.1078262>.
- Nayak, S., Takemi, T., 2019a. Dynamical downscaling of Typhoon Lionrock (2016) for assessing the resulting hazards under global warming. *J. Meteorol. Soc. Japan* 97, 69–88. <https://doi.org/10.2151/jmsj.2019-003>.
- Nayak, S., Takemi, T., 2019b. Quantitative estimations of hazards resulting from Typhoon Chanthu (2016) for assessing the impact in current and future climate. *Hydroclim. Res. Lett.* 13, 20–27. <https://doi.org/10.3178/hr.13.20>.
- Oke, T.R., 1988. Street design and urban canopy layer climate. *Energy Build.* 11, 103–113.
- Park, S.B., Baik, J.J., Han, B.S., 2015. Large-eddy simulation of turbulent flow in a densely built-up urban area. *Environ. Fluid Mech.* 15, 235–250.
- Ratti, C., Di Sabatino, S., Britter, R., Brown, M., Caton, F., Burian, S., 2002. Analysis of 3-D urban databases with respect to pollution dispersion for a number of European and American cities. *Water Air Soil Pollut. Focus* 2, 459–469.
- Raupach, M.R., 1992. Drag and drag partition on rough surfaces. *Bound.-Layer Meteorol.* 60, 375–395.
- Shao, Y., Yang, Y., 2005. A scheme for drag partition over rough surfaces. *Atmos. Env.* 39, 7351–7361.
- Shao, Y., Yang, Y., 2008. A theory for drag partition over rough surfaces. *J. Geophys. Res.* 113, F02S05.
- Takayabu, I., Kanamaru, H., Dairaku, K., Benestad, R., von Storch, H., Christensen, J.H., 2016. Reconsidering the quality and utility of downscaling. *J. Meteorol. Soc. Japan* 94A, 31–45. <https://doi.org/10.2151/jmsj.2015-042>.
- Takemi, T., 2013. High-resolution meteorological simulations of local-scale wind fields over complex terrain: A case study for the eastern area of Fukushima in March 2011. *Theor. Appl. Mech. Japan* 61, 3–10. <https://doi.org/10.11345/nctam.61.3>.

- Takemi, T., Ito, R., 2020. Benefits of high-resolution downscaling experiments for assessing strong wind hazard at local scales in complex terrain: A case study of Typhoon Songda (2004). *Progress in Earth and Planetary Science* 7, 4. <https://doi.org/10.1186/s40645-019-0317-7>.
- Takemi, T., Rotunno, R., 2003. The effects of subgrid model mixing and numerical filtering in simulations of mesoscale cloud systems. *Mon. Wea. Rev.* 131, 2085–2101.
- Takemi, T., Okada, Y., Ito, R., Ishikawa, H., Nakakita, E., 2016a. Assessing the impacts of global warming on meteorological hazards and risks in Japan: Philosophy and achievements of the SOUSEI program. *Hydrol. Res. Lett.* 10, 119–125. <https://doi.org/10.3178/hrl.10.119>.
- Takemi, T., Ito, R., Arakawa, O., 2016b. Effects of global warming on the impacts of Typhoon Mireille (1991) in the Kyushu and Tohoku regions. *Hydrol. Res. Lett.* 10, 81–87. <https://doi.org/10.3178/hrl.10.81>.
- Takemi, T., Ito, R., Arakawa, O., 2016c. Robustness and uncertainty of projected changes in the impacts of Typhoon Vera (1959) under global warming. *Hydrol. Res. Lett.* 10, 88–94. <https://doi.org/10.3178/hrl.10.88>.
- Takemi, T., Yoshida, T., Yamasaki, S., Hase, K., 2019. Quantitative estimation of strong winds in an urban district during Typhoon Jebi (2018) by merging mesoscale meteorological and large-eddy simulations. *SOLA* 15, 22–27. <https://doi.org/10.2151/sola.2019-005>.
- Tsuboki, K., Yoshioka, M.K., Shinoda, T., Kato, M., Kanada, S., Kitoh, A., 2015. Future increase of supertyphoon intensity associated with climate change. *Geophys. Res. Lett.* 42, 646–652.
- Vanderbauwhede, W., Takemi, T., 2015. Twinned buffering: A simple and highly effective scheme for parallelization of Successive Over-Relaxation on GPUs and other accelerators. In: High Performance Computing and Simulation (HPCS), 2015 International Conference on, 436–443, 20–24 July 2015, <https://doi.org/10.1109/HPCSim.2015.7237073>.
- Wieringa, J., 1993. Representative roughness parameters for homogeneous terrain. *Bound.-Layer Meteor.* 63, 323–363.
- Wyngaard, J.C., 2004. Toward numerical modeling in the «terra incognita». *J. Atmos. Sci.* 61, 1816–1826.
- Xie, Z.T., Coceal, O., Castro, I.P., 2008. Large-eddy simulation of flows over random urban-like obstacles. *Bound.-Layer Meteor.* 129, 1–23.
- Xu, X., Yang, Q., Yoshida, A., Tamura, Y., 2017. Characteristics of pedestrian-level wind around super-tall buildings with various configurations. *J. Wind Eng. Ind. Aerodyn.* 166, 61–73.
- Yoshida, T., Takemi, T., 2018. Properties of mixing length and dispersive stress in airflows over urban-like roughness obstacles with variable height. *SOLA* 14, 174–178. <https://doi.org/10.2151/sola.2018-031>.
- Yoshida, T., Takemi, T., Horiguchi, M., 2018. Large-eddy-simulation study of the effects of building height variability on turbulent flows over an actual urban area. *Bound.-Layer Meteor.* 168, 127–153.
- Zaki, S.A., Hagishima, A., Tanimoto, J., Ikegaya, N., 2011. Aerodynamic parameters of urban building arrays with random geometries. *Bound.-Layer Meteor.* 138, 99–120.
- Zhu, X., Iungo, G.V., Leonardi, S., Anderson, W., 2017. Parametric study of urban-like topographic statistical moments relevant to a priori modeling of bulk aerodynamic parameters. *Bound.-Layer Meteor.* 162, 231–253.